Icarus 331 (2019) 179–191

Contents lists available at ScienceDirect

Icarus

journal homepage: www.elsevier.com/locate/icarus

Boulder size and shape distributions on asteroid Ryugu

Tatsuhiro Michikami[a,*], Chikatoshi Honda[b], Hideaki Miyamoto[c], Masatoshi Hirabayashi[d], Axel Hagermann[e], Terunori Irie[a], Keita Nomura[a], Carolyn M. Ernst[f], Masaki Kawamura[a], Kiichi Sugimoto[a], Eri Tatsumi[g,h], Tomokatsu Morota[g,i], Naru Hirata[b], Takaaki Noguchi[j], Yuichiro Cho[g], Shingo Kameda[k], Toru Kouyama[l], Yasuhiro Yokota[m,o], Rina Noguchi[m], Masahiko Hayakawa[m], Naoyuki Hirata[n], Rie Honda[o], Moe Matsuoka[m], Naoya Sakatani[m], Hidehiko Suzuki[p], Manabu Yamada[q], Kazuo Yoshioka[g], Hirotaka Sawada[m], Ryodo Hemmi[r], Hiroshi Kikuchi[c], Kazunori Ogawa[n], Sei-ichiro Watanabe[i,m], Satoshi Tanaka[m], Makoto Yoshikawa[m], Yuichi Tsuda[m], Seiji Sugita[g,q]

[a] Faculty of Engineering, Kindai University, Hiroshima Campus, 1 Takaya Umenobe, Higashi-Hiroshima, Hiroshima 739-2116, Japan
[b] Graduate School of Computer Science and Engineering, University of Aizu, Tsuruga, Ikkimachi, Aizu Wakamatsu, Fukushima 965-8580, Japan
[c] Department of Systems Innovation, The University of Tokyo, 7-3-1 Hongo, Bunkyo, Tokyo 113-8656, Japan
[d] Department of Aerospace Engineering, Auburn University, 211 Davis Hall, Auburn, AL 36849-5338, United States
[e] Department of Biological and Environment Sciences, University of Stirling, FK9 4LA, Scotland, United Kingdom
[f] The Johns Hopkins University Applied Physics Laboratory, Laurel, MD 20723, United States
[g] Department of Earth and Planetary Science, Graduate School of Science, The University of Tokyo, 7-3-1 Hongo, Bunkyo, Tokyo 113-0033, Japan
[h] Instituto de Astrofisica de Canrias, Calle Vía Láctea, s/n, 38205 San Cristóbal de La Laguna, Santa Cruz de Tenerife, Spain
[i] Graduate School of Environmental Studies, Nagoya University, Furo-cho, Chikusa-ku, Nagoya 464-8601, Japan
[j] Faculty of Arts and Science, Kyushu University, 744 Motooka, Nishi-ku, Fukuoka 819-0395, Japan
[k] College of Science, Rikkyo University, 3-34-1 Nishi-Ikebukuro, Toshima, Tokyo 171-8501, Japan
[l] Artificial Intelligence Research Center, National Institute of Advanced Industrial Science and Technology, 2-3-26, Aomi, Koto-ku, Tokyo 135-0064, Japan
[m] Institute of Space and Astronautical Science (ISAS), Japan Aerospace Exploration Agency (JAXA), 3-1-1 Yoshinodai, Chuo, Sagamihara 252-5210, Japan
[n] Graduate School of Science, Kobe University, Kobe, 1-1 Rokkodaicho, Nada, Kobe, Hyogo 657-8501, Japan
[o] Faculty of Science and Technology, Kochi University, 2-5-1 Akebono-cyo, Kochi 780-8520, Japan
[p] Department of physics, Meiji University, Kawasaki, 1-1-1 Higashimita, Tama-ku, Kawasaki 214-8571, Japan
[q] Planetary Exploration Research Center, Chiba Institute of Technology, 2-17-1 Tsudanuma, Narashino 275-0016, Japan
[r] The University Museum, The University of Tokyo, 7-3-1 Hongo, Bunkyo-ku, Tokyo 113-0033, Japan

ARTICLE INFO

Keywords:
Asteroids
Surfaces
Impact processes
Geological processes
Asteroid Ryugu
Regoliths

ABSTRACT

In 2018, the Japanese spacecraft Hayabusa2, arrived at the small asteroid Ryugu. The surface of this C-type asteroid is covered with numerous boulders whose size and shape distributions are investigated in this study. Using a few hundred Optical Navigation Camera (ONC) images with a pixel scale of approximately 0.65 m, we focus on boulders greater than 5 m in diameter. Smaller boulders are also considered using five arbitrarily chosen ONC close-up images with pixel scales ranging from 0.7 to 6 cm.

Across the entire surface area (~2.7 km^2) of Ryugu, nearly 4400 boulders larger than 5 m were identified. Boulders appear to be uniformly distributed across the entire surface, with some slight differences in latitude and longitude. At ~50 km^{-2}, the number density of boulders larger than 20 m is twice as large as on asteroid Itokawa (or Bennu). The apparent shapes of Ryugu's boulders resemble laboratory impact fragments, with larger boulders being more elongated. The ratio of the total volume of boulders larger than 5 m to the total excavated volume of craters larger than 20 m on Ryugu can be estimated to be ~94%, which is comparatively high. These observations strongly support the hypothesis that most boulders found on Ryugu resulted from the catastrophic disruption of Ryugu's larger parent body, as described in previous papers (Watanabe et al., 2019; Sugita et al., 2019).

The cumulative size distribution of boulders larger than 5 m has a power-index of -2.65 ± 0.05, which is comparatively shallow compared with other asteroids visited by spacecraft. For boulders smaller than 4 m, the power-index is even shallower and ranges from -1.65 ± 0.05 to -2.01 ± 0.06. This particularly shallow

* Corresponding author.
E-mail address: michikami@hiro.kindai.ac.jp (T. Michikami).

https://doi.org/10.1016/j.icarus.2019.05.019
Received 28 January 2019; Received in revised form 9 May 2019; Accepted 17 May 2019
Available online 21 May 2019

power-index implies that some boulders are buried in Ryugu's regolith. Based on our observations, we suggest that boulders near the equator might have been buried by the migration of finer material and, as a result, the number density of boulders larger than 5 m in the equatorial region is lower than at higher latitudes.

1. Introduction

Boulders on an asteroid provide an opportunity to study the physical properties and the geological evolution of the asteroid's surface, as well as its collisional history as evidenced by craters. In general, boulders are produced either by impact cratering or catastrophic disruption of the parent body, or a combination of the two. For instance, most boulders on relatively large asteroids, such as Eros (34 × 11 × 11 km; Veverka et al., 2000) and Ida (59.8 × 25.4 × 18.6 km; Belton et al., 1996), are considered to be the products of impact cratering (Lee et al., 1996; Thomas et al., 2001). On the other hand, most boulders on relatively small asteroids, such as Itokawa (0.535 × 0.294 × 0.209 km; Fujiwara et al., 2006), Bennu (0.565 × 0.536 × 0.498 km; Lauretta et al., 2019) and Toutatis (~4.6 × 2.3 × 1.9 km; Huang et al., 2013), are considered to be the products of catastrophic disruption of their parent bodies (Fujiwara et al., 2006; Michikami et al., 2008; Jiang et al., 2015; Michel and Richardson, 2013; DellaGiustina et al., 2019).

The recent exploration of near-Earth asteroid Ryugu by the Japan Aerospace Exploration Agency's (JAXA) Hayabusa2 spacecraft yielded the first high-resolution images of the surface of a C-type asteroid. The size of Ryugu (1.04 × 1.02 × 0.88 km, Watanabe et al., 2019) is intermediate between Itokawa (or Bennu) and Toutatis. Images taken by the optical navigation cameras (ONCs; Kameda et al., 2017) on board the Hayabusa2 spacecraft showed that Ryugu is covered with a large number of boulders, whose appearance is somehow similar to those on Itokawa. The bulk density of Ryugu is 1190 ± 20 kg/m^3, which implies high porosity (> 50%) for a carbonaceous asteroid (Watanabe et al., 2019). The existence of numerous boulders and the derived high porosity of Ryugu indicate that Ryugu is a rubble-pile asteroid (Watanabe et al., 2019; Sugita et al., 2019). These observations support the theory that most small asteroids in the size range from sub-km to km are rubble piles, and most boulders on these asteroids may be fragments that formed by catastrophic disruption of their parent bodies. That is, the existence of numerous boulders on small asteroids is considered to be common. For instance, asteroid Bennu, recently explored by NASA's OSIRIS-REx mission, also has numerous boulders on the surface (Lauretta et al., 2019). Boulder counting provides critical constraints on the formation and evolution of these asteroids.

The purpose of this study is to analyze the boulders on the surface of Ryugu quantitatively and discuss the formation and evolution of Ryugu. To this end, we investigate the size distribution, the spatial distribution and the shape distribution of numerous boulders on Ryugu based on images taken by the Hayabusa2 spacecraft.

2. Methodology

Wentworth (1922) defined blocks of 4–64 mm as pebbles, 64–256 mm as cobbles, and > 256 mm as boulders, respectively. In this paper, we define a boulder as an isolated positive relief feature with a size larger than 256 mm on the surface of an asteroid. Boulders on Ryugu show various geomorphological characteristics. Some have distinguished outlines relatively easy to trace, while others are partially buried or weathered with obscured outlines. Some appear as piles of gravel or a part of a geologic feature such as protruding bedrocks, raised crater rims, or intersecting crater walls. The number of ONC close-up images is limited, but they clearly show some boulders are largely buried in the finer particles of the regolith layer. In fact, there are considerably more partially buried boulders on Ryugu than there are on Itokawa. This makes it difficult to identify geomorphological variations of boulders from Hayabusa's nominal hovering position (a.k.a. home position) at an altitude of about 20 km. Thus, in order to obtain the size distribution of boulders on the entire surface of Ryugu, we analyze ONC images taken by the spacecraft at an altitude of about 6.5 km (resolutions ~0.65 m/pixel) on 20th July 2018. We extract the features that help identify a boulder by comparing multiple images stereographically. We also study small boulders, cobbles and pebbles with sizes of 0.02 to 9.1 m from close-up images of narrower localities taken at altitudes from 67 m to 620 m on 21th September 2018. The locations of the areas considered and corresponding results are described in Section 3.3.

Boulders larger than 2 m are mapped on a global scale and are measured on the shape models of Ryugu (SFM20180804; Watanabe et al., 2019) using the Small Body Mapping Tool (SBMT; Mazrouei et al., 2014; Ernst et al., 2018). Boulders are mapped out as ellipses, where the semi-major and semi-minor axes provide a long and short axis for each boulder. In this study, the mean horizontal dimension of a boulder is defined as the arithmetic mean of these two axes. Note that

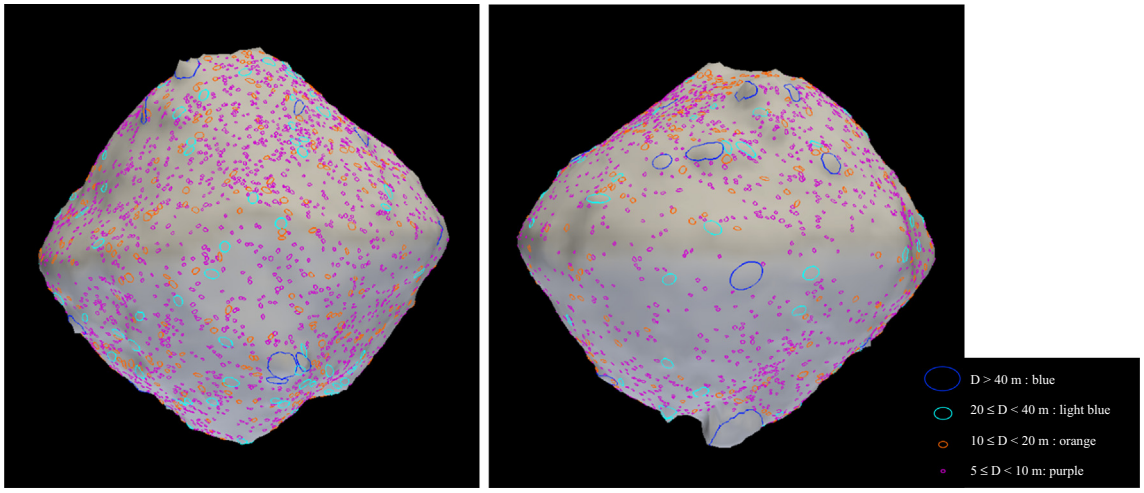

Fig. 1. Location of mapped boulders larger than 5 m in diameter on the surface of Ryugu observed near 90° E (left) and 270° E (right) longitude.

this study extends the boulder counting by Sugita et al. (2019), who defined the size of a boulder as the maximum dimension of the positive relief features on the surface.

On five close-up images on the SAOImage DS9, small boulders, cobbles and pebbles with sizes of 0.02 to 9.1 m are mapped, and their sizes determined.

Note that there is observational bias on the global mapping of boulders; boulder mapping is affected by variations in spatial resolution and in the availability of stereographic coverage. The regions in the mid and low latitudes are viewed from hundreds of images at resolution ~0.65 m/pixel and with substantial stereo coverage. On the other hand, high latitude regions are viewed from only several images at resolution ~2 m/pixel and with no stereo coverage. Therefore, some boulders located at high latitude are not taken into account in our data.

3. Observational results

3.1. Global boulder size distribution

Nearly 9700 boulders larger than 2 m in diameter were measured and a total of ~4400 boulders larger than 5 m were observed over the entire surface area of ~2.7 km^2 (Fig. 1). The spatial resolution of the entire asteroid surface imaged by the spacecraft imposes no restrictions on the critical size of 5 m. Fig. 2a shows the cumulative boulder size distribution per unit area across the entire surface of Ryugu. Importantly, the number density of boulders larger than 20 m on Ryugu is ~50 km^{-2}, which is twice as large as that (~25 km^{-2}) on Itokawa (Mazrouei et al., 2014) or that (~28.2 km^{-2}) on Bennu (DellaGiustina et al., 2019). To help highlight minor variations in the size distribution within narrow size ranges, the R-plot size-frequency data for boulders larger than 5 m on the entire surface of Ryugu is shown in Fig. 2b. Boulders larger than 40 m are rare on Ryugu.

The largest boulder, whose size is ~160 × 120 × 70 m, is located near the south pole and is called “Otohime”. This size is too large for it to be considered a part of ejecta even from the largest crater of Ryugu (Sugita et al., 2019; Cho et al., 2019; Morota et al., 2019). The size ratio of the largest boulder (mean horizontal dimension ~140 m) to the largest crater (300 m) on Ryugu is ~47%, which is extremely high. By comparison, on small asteroid Itokawa, the size ratio of the largest boulder (40 m; Saito et al., 2006) to largest crater (134 m; Hirata et al., 2009) is ~30%. Moreover, on Bennu, the size ratio of the largest boulder (longest dimension ~56 m; Walsh et al., 2019) to largest crater (150 m; Walsh et al., 2019) is ~37%. These are considered significantly high, and thus, most boulders on Itokawa and Bennu are considered to be the products of the catastrophic disruption of the parent body (e.g. Michikami et al., 2008; Walsh et al., 2019). On the contrary, on the relatively large asteroid Eros, the ratio of the largest boulder (150 m) to the largest crater (7600 m) is very low, ~2% (Thomas et al., 2001). Most boulders on Eros are considered to be the products of the impact cratering (Thomas et al., 2001). Regarding the size of the largest boulder originated from impact cratering, earlier work (e.g. Lee et al., 1996; Thomas et al., 2001) showed correlations between the largest boulder size (L) and the source crater diameter (D_c) for the Moon, the Martian satellites (Phobos and Deimos), and asteroids Ida and Eros. One of the empirical relationships is expressed as $L \sim 0.25\ D_c{}^{0.7}$, with L and D_c in meters (Lee et al., 1996). For Ryugu, this relationship is not applicable because the largest boulder is relatively large compared with the largest crater. Therefore, the size ratio of the largest boulder to the largest crater on Ryugu suggests that most boulders on Ryugu are surviving fragments from the parent body of Ryugu, accreted after its breakup.

The power-index of the cumulative boulder size distribution per unit area of Ryugu is obtained by combining a maximum-likelihood fitting method with goodness-of-fit tests based on the Kolmogorov-Smirnov statistic and likelihood ratios (Clauset et al., 2009; Tancredi et al., 2015). We find that the power-index of Ryugu's boulders is -2.65 ± 0.05, which is consistent with an initial estimate of -2.5 to -3 by Sugita et al. (2019).

The slope of -2.65 on Ryugu is less steep than on Itokawa (-3.1 ± 0.1: Michikami et al., 2008; -3.3 ± 0.1: Mazrouei et al., 2014) and other asteroids visited by spacecraft (The range of observed power-index of the boulder size distributions on asteroids is clustered between -3 to -4 (e.g. Bart and Melosh, 2010)) except for Bennu. The power-index of Bennu's boulders larger than 8 m (longest dimension) is -2.9 ± 0.3 (DellaGiustina et al., 2019). This is similar to the power-index of Ryugu's boulders which, for the longest dimension, is

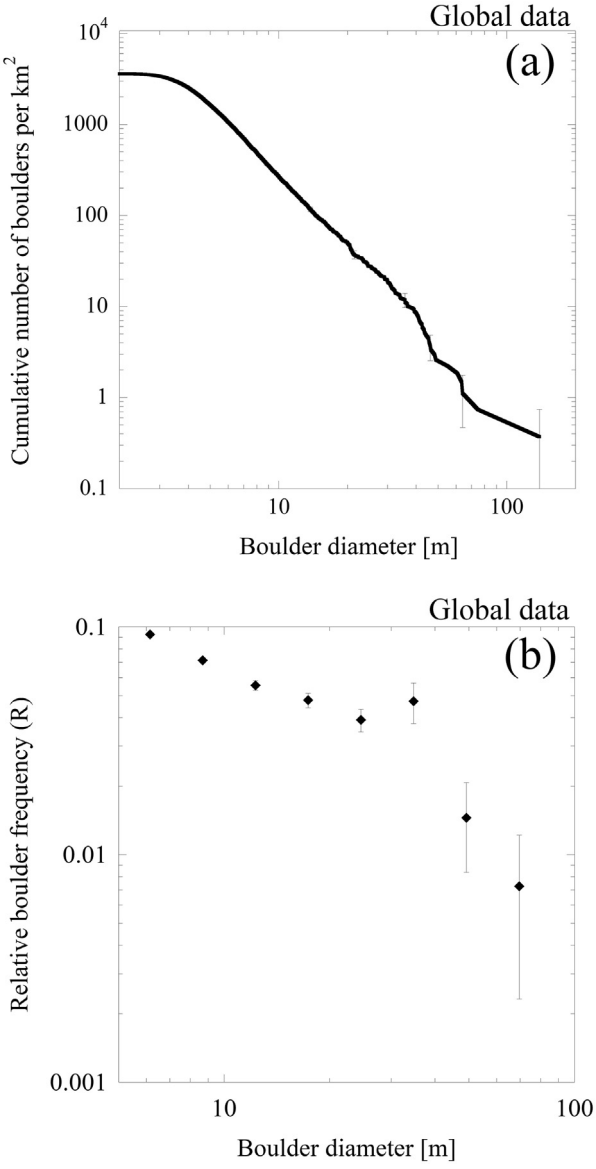

Fig. 2. (a) Cumulative boulder size distribution per unit area on the entire surface of Ryugu. The horizontal axis shows the diameter of the boulders, where diameter is defined as the mean horizontal dimension of the boulder. The vertical axis shows the number of boulders larger than a particular diameter per unit area. Vertical error bars indicate the root of the cumulative number of boulders counted, divided by total area (2.7 km^2) of Ryugu. The error bars are given only for a few points to make the figure legible. The power-index of the size distribution is -2.65 ± 0.05, which is less steep compared with other asteroids visited by spacecraft.
(b) An R-plot size-frequency data for boulders larger than 5 m on the entire surface of Ryugu (R is the differential size-frequency divided by D^{-3}, where D is boulder diameter; error bars reflect counting statistics only, not any systematic errors).

Table 1
Regions investigated and observational results of boulders on Ryugu with Itokawa data added. The power-index of cumulative boulder size distributions as the minimum diameters ($D_{\min}$) are obtained combining a maximum-likelihood fitting method with goodness-of-fit tests based on the Kolmogorov-Smirnov statistic, as mentioned by Clauset et al. (2009) and Tancredi et al. (2015). The cumulative boulder size distribution is expressed by $N(>D) = CD^{-\alpha}$, where D is the boulder diameter, α is the power-index and C is a constant.

The maximum-likeihood indicator of the power-index α can be calculated by

$$\alpha = \frac{n}{\sum_{i=1}^{n} ln \frac{D_i}{D_{min}}},$$

where D_i, $i = 1,2,3,\cdots n$, are the observed values of the diameters ($D_i \geq D_{min}$), and n is the total number of boulders larger than $D_{\min}$. In order to obtain the minimum diameter, we compute the Kolmogorov-Smirnov statistic for different values of D_{min}, which is simply the maximum distance between the data of the cumulative size distribution and the fitted model; the estimate D_{min} is the value of D_{min} that minimises this distance (Tancredi et al., 2015).

Asteroid	Region	Image	Counted number of boulders	$D_{\min}$ [m]	Number fitting	Power-index α	Error bar of α	Size range [m]	Mean b/a ratio
Ryugu	Global data		9691	5.8	3153	2.65	0.05	2–140	0.70
	Close-up (b)	hyb2_onc_20180921_043010_tvf_l2c.fit	2581	0.46	1301	2.07	0.06	0.2–9.1	0.71
	Close-up (c)	hyb2_onc_20180921_041826_tvf_l2c.fit	2808	0.26	1321	2.01	0.06	0.1–4.1	0.70
	Close-up (d)	hyb2_onc_20180921_034938_tvf_l2c.fit	2004	0.17	721	1.96	0.07	0.05–3.37	0.68
	Close-up (e)	hyb2_onc_20180921_040154_tvf_l2c.fit	1363	0.09	492	1.98	0.09	0.02–1.83	0.68
	Close-up (f)	hyb2_onc_20180921_040634_tvf_l2c.fit	1738	0.04	1087	1.65	0.05	0.02–3.26	0.69
Itokawa	Global data of Mazrouei et al. (2014)		1438	7.52	318	3.52	0.20	2–38	0.65
	Global data of Michikami et al. (2010)		373	–	–	–	–	5–40	0.62
	Close-up (b) in Fig. 1 of Michikami et al. (2010)	ST2539437177	276	–	–	–	–	0.12–4.65	0.67
	Close-up (c) in Fig. 1 of Michikami et al. (2010)	ST2539429953	410	–	–	–	–	0.22–3.84	0.67
	Close-up (d) in Fig. 1 of Michikami et al. (2010)	ST2539423137	439	–	–	–	–	0.23–2.74	0.66
	Close-up (e) in Fig. 1 of Michikami et al. (2010)	ST2532629277	495	–	–	–	–	0.58–5.37	0.68
	Close-up (f) in Fig. 1 of Michikami et al. (2010)	ST2539451609	173	–	–	–	–	0.14–2.15	0.69
	Close-up (g) in Fig. 1 of Michikami et al. (2010)	ST2539444467	240	–	–	–	–	0.05–2.56	0.69
	Close-up (b)-(g) in Fig. 1 of Michikami et al. (2010)		2033	–	–	–	–	0.05–5.37	0.68

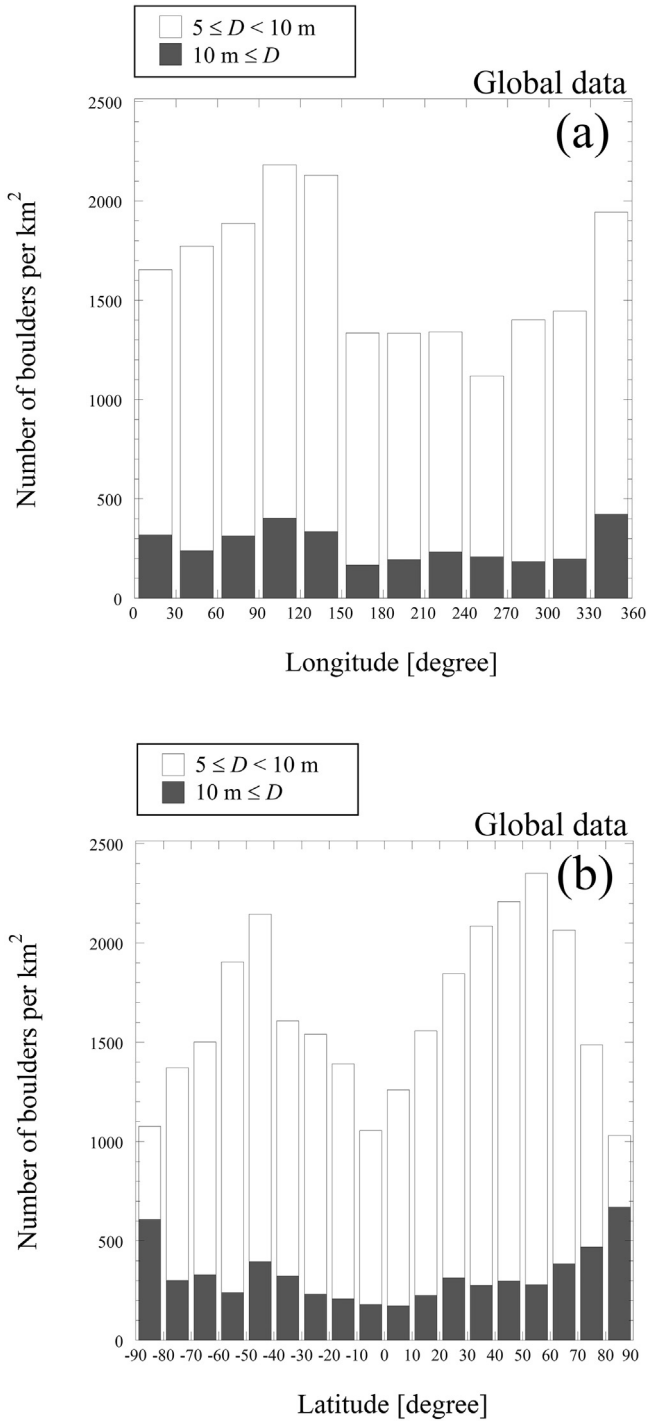

Fig. 3. (a) Histogram of boulder surface density for two different size ranges (5–10 m and ≥ 10 m in diameter) as a function of longitude on Ryugu. (b) Histogram of boulder surface density for two different size ranges (5–10 m and ≥ 10 m in diameter) as a function of latitude on Ryugu.

-2.62 ± 0.05.

In general, a power-index steeper than -2 is indicative of very fragmented material, and a steeper index is further indicative of greater degree of fragmentation (Hartmann, 1969; Thomas et al., 2001). In this sense, boulders on Ryugu might have experienced a lesser degree of fragmentation compared with other asteroids. However, the number density of large boulders > 20 m on Ryugu is twice as large as on Itokawa (or Bennu), and the number density of boulders > 10 m on Ryugu is larger than on any other asteroids such as Eros, Itokawa and Toutatis. Such a high number density of large boulders strongly suggest that Ryugu's boulders were formed due to heavy fragmentation during its parent body's catastrophic disruption. Significantly, close-up images indicate some boulders are buried in the regolith layer (e.g. Fig. 4(e)). The number of buried boulders is likely to increase as the boulder size decreases. Taking this burial effect into account, the power-index of Ryugu would become less steep.

Note that the power-index of the boulder size distribution changes depending on the methods used for measurement, analysis and statistics. Saito et al. (2006) used the maximum dimension of each boulder as its size and found a power-index of -2.8. On the other hand, Michikami et al. (2008) analyzed boulder size using the mean horizontal dimension and obtained a power-index of -3.1. This difference results from the definition of boulder size (the long shapes of the boulders affect their power-indices). Mazrouei et al. (2014) performed a more detailed study of the size distribution of Itokawa's boulders > 6 m and showed that the power-index is -3.3 if the mean horizontal dimension is used, with the difference to Michikami et al. (2008) being due to the analysis method, i.e. DS9 vs. SBMT.

Finally, we need to confirm our conclusions are not affected by our choice of statistical methods. Clauset et al. (2009) pointed out that commonly used methods for analyzing power-law data, such as least-squares fitting, can produce substantially inaccurate estimates of parameters in a power-law distribution. They recommend an approach which combines a maximum-likelihood fitting with goodness-of-fit tests based on the Kolmogorov-Smirnov statistic and likelihood ratios. Michikami et al. (2008) and Mazrouei et al. (2014) estimated the power-index of the cumulative boulder size distribution of Itokawa by applying least-squares fitting in the log-log plot. Thus, in order to compare our data of Ryugu with that of Itokawa quantitatively, it is necessary to re-estimate the power-index of Itokawa by the same statistical method of Clauset et al. (2009). We compute the power-index of Itokawa by using the raw data of Fig. 3(b) in Mazrouei et al. (2014) and show that the power-index of Itokawa is -3.52 ± 0.20 (Table 1), which is slightly steeper than the value estimated by Mazrouei et al. (2014). This updated power-index does not change the observation that the power-index of Ryugu is less steep than Itokawa.

3.2. Boulder spatial distributions

Ryugu is a top-shaped asteroid that is symmetric along its axis of rotation, with an oblate shape, and a circular equatorial ridge of 502-meter radius (Watanabe et al., 2019). A similar shape is also seen in Bennu (Lauretta et al., 2019). As indicated before, the spatial distribution of boulders larger than 5 m is given in Fig. 1. Unlike Itokawa, which has clearly visible smooth areas, Ryugu's (and Bennu's: e.g. Walsh et al., 2019) entire surface appears to be rough and covered with numerous boulders. The spatial distribution of boulders larger than 5 m appears to be generally uniform, regardless of the locations of large craters. This is important because boulders that originated from impact cratering are usually located near their source craters; for instance, the boulders on Ida lie within or near the rims of the Lascaux and Mammoth craters (Lee et al., 1996), and most boulders on Eros are located near Shoemaker crater which has a diameter of 7.6 km (Thomas et al., 2001). On the other hand, boulders originated from catastrophic disruption of a parent body, can be almost randomly distributed - although their distribution critically depends on the re-accretion mechanism. Most boulders on Itokawa are relatively uniformly distributed over the entire surface, with only a slight difference in the rough and smooth areas (e.g. Michikami et al., 2008). Thus, the uniform distribution of boulders on Ryugu implies that most boulders on this asteroid might have originated from catastrophic disruption of Ryugu's parent body.

Note that Walsh et al. (2019) suggest that the spatial distribution of boulders on the surface of the rubble pile asteroid Bennu is not uniform. However, this suggestion is based on the data of boulders which are relatively large (> 8 m) compared with the size of Bennu. In general,

the number density of relatively large boulders shows some scatter because there are only few in each area. This indicates that further observations for small boulders might be required in order to better understand the spatial distributions of boulders on the surface of Bennu.

Next, we discuss the distributions of boulders as a function of longitude and latitude. Fig. 3a shows the histograms of distributions of boulders in two different size ranges (5–10 m and ≥10 m in diameter) as a function of longitude. The boulders in a given longitude bin are normalized by the corresponding surface area of Ryugu in that bin. The shapes of the histograms are similar regardless of size ranges, indicating that the power-indices of the boulder size distributions by longitude are similar. The longitude distribution in Fig. 3a exhibits two peaks at longitudes 90°–120°E and 330°–360°E. The western hemisphere (160°–290°E), surrounded by troughs, as shown by Sugita et al. (2019), has a relatively lower boulder density compared with the rest of the surface (Hirabayashi et al. (2019) explores a possible structural formation process of this longitudinal dichotomy). However, the number density of the boulders ≥5 m in each bin differs by only a factor of two. On Eros, however, the boulder number densities for a particular size differ by more than an order of magnitude at different locations (Thomas et al., 2001). Thus, when compared with Eros, the boulder number density of Ryugu as a function of longitude can be considered

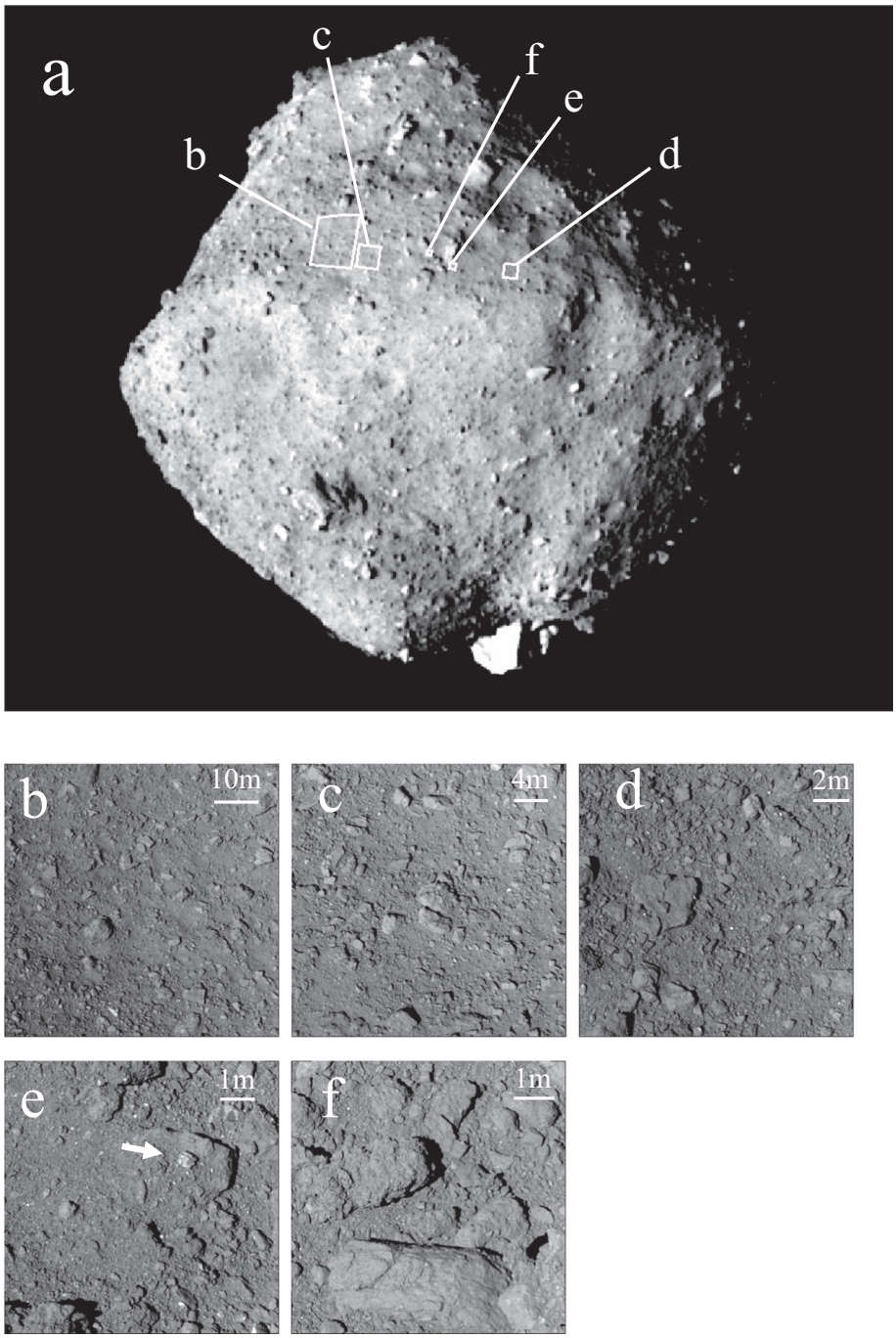

Fig. 4. (a) Ryugu near 130° E (hyb2_onc_20180630_130943_tvf_l2c.fit). (b-f) Close-up images acquired on 21th September 2018. Scale bars are indicated on the top right of each images. Image IDs: (a) hyb2_onc_20180630_130943_tvf_l2c.fit, (b) hyb2_onc_20180921_043010_tvf_l2c.fit, (c) hyb2_onc_20180921_041826_tvf_l2c.fit, (d) hyb2_onc_20180921_034938_tvf_l2c.fit, (e) hyb2_onc_20180921_040154_tvf_l2c.fit, (f) hyb2_onc_20180921_040634_tvf_l2c.fit. The locations of the regions covered by images (b-f) are shown in (a). Arrow in (e) indicates a part of the boulder is buried in finer particles.

to be comparatively uniform.

Fig. 3b shows the histogram of boulders in two different size ranges (5–10 m and ≥10 m in diameter) as a function of latitude. Near the poles, the shapes of the histograms are different in the two size ranges. Note that the small number of data points for boulders located north of 60°N and south of 60°S may be insufficient for rigorous statistical treatment. We can only state that the boulder number density in the equatorial region is lower than at higher latitudes as already pointed out by Sugita et al. (2019). In contrast, on Itokawa, the number density of the boulders is higher in the equatorial region than at higher latitudes (Mazrouei et al., 2014). One possible explanation for the difference between Itokawa and Ryugu could be the existence of buried boulders in the equatorial region of Ryugu. We discuss this possibility in Section 4.2.

3.3. Small boulder size distributions on five close-up images

Fig. 4 shows five close-up images and their context. They were taken at spacecraft altitudes from 67 to 620 m on 21th September 2018 (at latitudes from 10°N to 20°N), before and after releasing the MINERVA-II landers from Hayabusa2. Small boulders, cobbles and pebbles with sizes of 0.02 to 9.1 m are measured from these images. Fig. 5a and b show the size distributions and the R-plot size frequency data of small boulders (including cobbles and pebbles) in five close-up images, respectively. We found a few thousand small boulders in each image. Fig. 5b indicates that the number densities of these small boulders are high, implying the surface is close to the saturation with boulders. The size distributions in Fig. 5a appear to overlap and form a straight line. However, the power-index of each size distribution is slightly different. The power-index of the boulder size distribution for each image is also derived by the approach suggested by Clauset et al. (2009) (Table 1). The results indicate that the slope (the power-index) of the size distribution gradually decreases with decreasing boulder size. The power-index of the size distribution of small boulders with sizes of 0.1–4.1 m (Fig. 4c), and with sizes of 0.02–3.26 m (Fig. 4f) are -2.01 ± 0.06 and -1.65 ± 0.05, respectively. This implies that some boulders are buried in finer particles, which will be discussed in Section 4.2.

3.4. Boulder shape distributions

The boulder shape distribution also provides information related to the formation of the boulders on the surface. According to Michikami et al. (2016), in laboratory impact experiments, the shapes of fragments defined by the maximum dimensions of the impact fragments in three mutually orthogonal planes ($a \geq b \geq c$) are strongly dependent on the degree of fragmentation of the target. Specifically, the mean c/a ratios of the relatively large fragments gradually decrease with decreasing impact energy per unit target mass; in other words, the relatively large fragments produced by low-energy impact cratering tend to have flat shapes while those produced by catastrophic disruption have oblate shapes. On the other hand, the mean b/a ratios of the fragments are almost constant, independent of experimental conditions such as the degree of fragmentation, target shape, composition and strength (Although Ryugu's porosity is high, the above rule regarding fragment shapes would be applicable to Ryugu's boulders. This is because impact experiments show that the fragment shapes from catastrophic disruptions of porous targets (a mortar target with 40% porosity) and non-porous targets are similar (Michikami, 2012)).

First, we investigate the apparent b/a ratios of all the observed boulders on Ryugu. Then, we choose some boulders to measure their apparent b/a and c/a by assuming that boulders' apparent height above the surface represent their c axes. The dimensions of the c axes are derived from images with a viewing angle rotated by 90° with respect to the image used for determining the dimensions of the a and b axes (i.e. c axes are determined by their protrusions of the boulders located at the edge of the image).

Fig. 6 shows the histogram of the apparent b/a ratios of boulders with sizes 2 to 140 m across the surface of Ryugu. In the study, boulders located north of 60°N and south of 60°S are excluded because their shapes may not represent the real shapes owing to difficulties in making

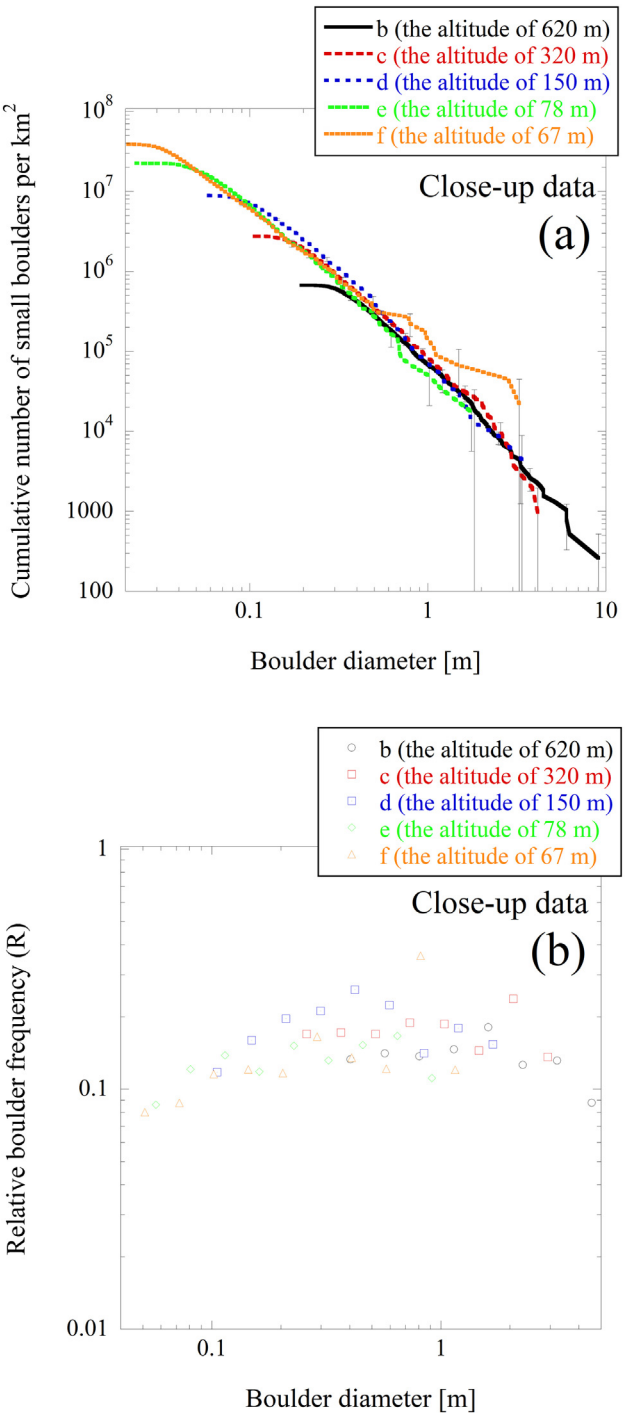

Fig. 5. (a) Cumulative small boulder size distribution (which includes cobbles and pebbles) per unit area in five close-up images on 21th September 2018. Vertical error bars indicate the root of the cumulative number of boulders divided by the corresponding area on Ryugu. Error bars are restricted to only a few points to improve legibility. The power-index for each size distribution is shown in Table 1. The distance between the spacecraft and the surface of Ryugu is given in parentheses.
(b) An R-plot size-frequency data for small boulders in five close-up images on 21th September 2018 (see caption to Fig. 2b). The error bars are smaller than the size of each symbol.

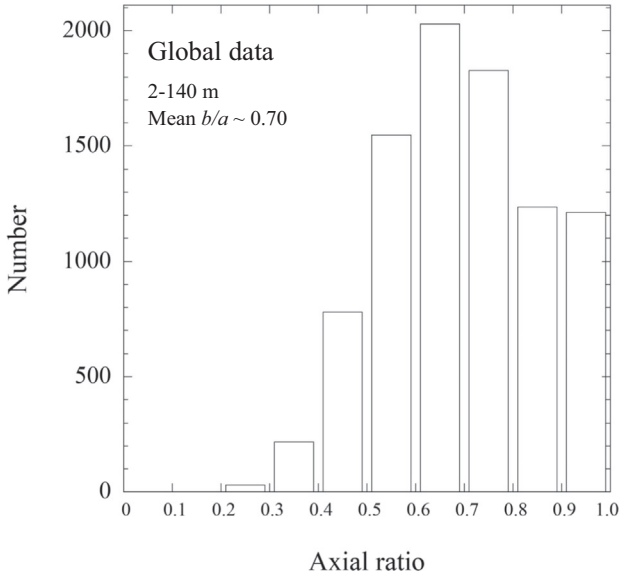

Fig. 6. Histograms of apparent axial ratios (b/a) of the counted boulders across the surface of Ryugu except for boulders located north of north of 60°N and south of 60°S. The size range and mean b/a ratio of the boulders are indicated.

the measurements at high latitudes (We have, however, confirmed that these shape inaccuracies do not significantly influence the boulder size distribution). We excluded nearly 800 of the boulders. This constitutes, however, only ~8% of the total number counted, so the influence of the boulders excluded on the apparent b/a ratios of the total would be negligible.

The result shows that the apparent mean b/a ratio of boulders > 2 m is 0.70, which is similar to the ratios of laboratory impact fragments, which lie in the range 0.70–0.74 (Fujiwara et al., 1978; Capaccioni et al., 1984, 1986; Michikami et al., 2016, 2018). The apparent b/a ratios of boulders on Ryugu have a peak at 0.6–0.7, which is slightly smaller than laboratory impact fragments (0.7–0.8) (Fujiwara et al., 1978; Capaccioni et al., 1984, 1986; Michikami et al., 2016, 2018). In particular, there are relatively few fragments with $b/a < 0.4$ in laboratory experiments, while there are several hundreds of boulders with $b/a < 0.4$ on Ryugu.

On Itokawa, there is a difference in shape between large and small boulders (Table 1): the apparent mean b/a ratio is 0.62 for boulders larger than 5 m while it is 0.68 for those boulders smaller than 5 m (For the sake of accuracy, note that the former is derived from observations of the entire surface of Itokawa while the latter considers several local areas (Michikami et al., 2010)). On Ryugu, the apparent mean b/a ratio of boulders > 5 m is 0.68, which is slightly smaller than the ratio of boulders > 2 m: 0.70. In order to investigate the effect of the boulder size on the boulder shapes for Ryugu we use the same data from Fig. 6, plotting a running-box diagram of apparent mean b/a ratio vs boulder mean size (Fig. 7). The boulders have been ordered by size and grouped into bins of 200 fragments each. There are clear fluctuations of the apparent mean b/a ratios, which merely reflect the fact that there are numerous small boulders, and fewer large boulders (Michikami et al., 2016). The apparent mean b/a ratio of the boulders increases as the boulder diameter decreases. At smaller size the apparent mean b/a ratios are similar to or greater than 0.70, similar to laboratory impact fragment ratios (although the apparent mean b/a of boulders smaller than 4 m might not reflect their real shape because of limited image resolution). On the other hand, at larger size the apparent mean b/a ratios are nearly 0.67, slightly less than laboratory impact fragment ratios.

Fig. 8, which uses the data obtained from the five close-up images in Fig. 5, shows the histograms of the apparent b/a ratios of the small boulder with sizes of 0.02 to 9.1 m. The results show that the mean apparent b/a ratios of these small boulders range from 0.68 to 0.71, values similar to laboratory impact fragments and boulders smaller than 5 m on Itokawa.

Fig. 9a shows that the apparent mean b/a ratios of boulders with three different size ranges (≥2 m, ≥5 m and ≥10 m in diameter) as a function of longitude using the same data as Fig. 6. The apparent mean b/a ratios appear to be approximately constant, regardless of longitude. On the other hand, the apparent mean b/a ratios seem to depend on latitude of Ryugu (Fig. 9b). Fig. 9b shows that the apparent mean b/a ratios of the boulders with three different size ranges (≥2 m, ≥5 m and ≥10 m in diameter) as a function of latitude, again using the same data set. The apparent mean b/a ratio has a maximum near the equator and a lower peak near 60°N, independent of size range. The same caveat as above applies for boulders located near 60°N and 60°S. Because there are fewer images at high latitudes, data are sparse and boulder shapes may be distorted compared with the boulders at low latitudes. Therefore, in Fig. 9b, we can only state that the apparent mean b/a ratio in the equatorial region is larger than at higher latitudes, which suggests a migration of boulders as described in Section 4.2.

A diagram of b/a and c/a of 121 arbitrarily selected boulders obtained from a few hundred images on 20th July 2018 is shown in Fig. 10a. We selected only boulders whose heights are easily detected by eye in the limited spatial resolution on the entire surface. The mean apparent axial b/a and c/a ratios are 0.71 and 0.44, respectively. According to Michikami et al.'s (2016) impact experiments, mean c/a ratio around 0.44 is indicative of fragments resulting from catastrophic disruption. This implies that the parent body of Ryugu is likely to have experienced a catastrophic rather than a weak disruption. However, note that only a limited number of boulders have been chosen to measure the shape and the entire process may include observational biases that affect computation of the b/a and c/a ratios. For instance, the power-index of the cumulative size distribution of the selected boulders is -1.24 ± 0.12 (Fig. 10b), which is significantly less steep than the value for all boulders counted across the entire surface of Ryugu (Fig. 1). Therefore, further investigation is necessary to quantify the shape distribution of boulders, which constrains the origin and evolution of boulders on Ryugu.

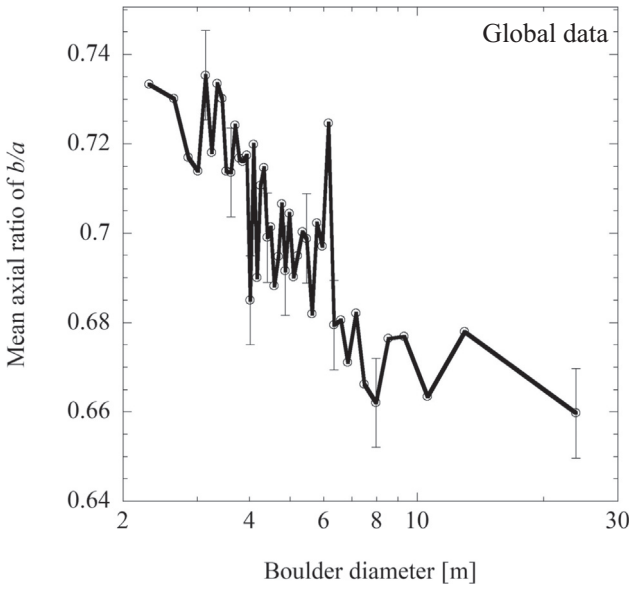

Fig. 7. Running box diagram of the mean b/a ratios in each bin including 200 boulders vs the boulder mean diameter, which are the same data presented in Fig. 6. The error bars are given only for a few points to make the figure legible.

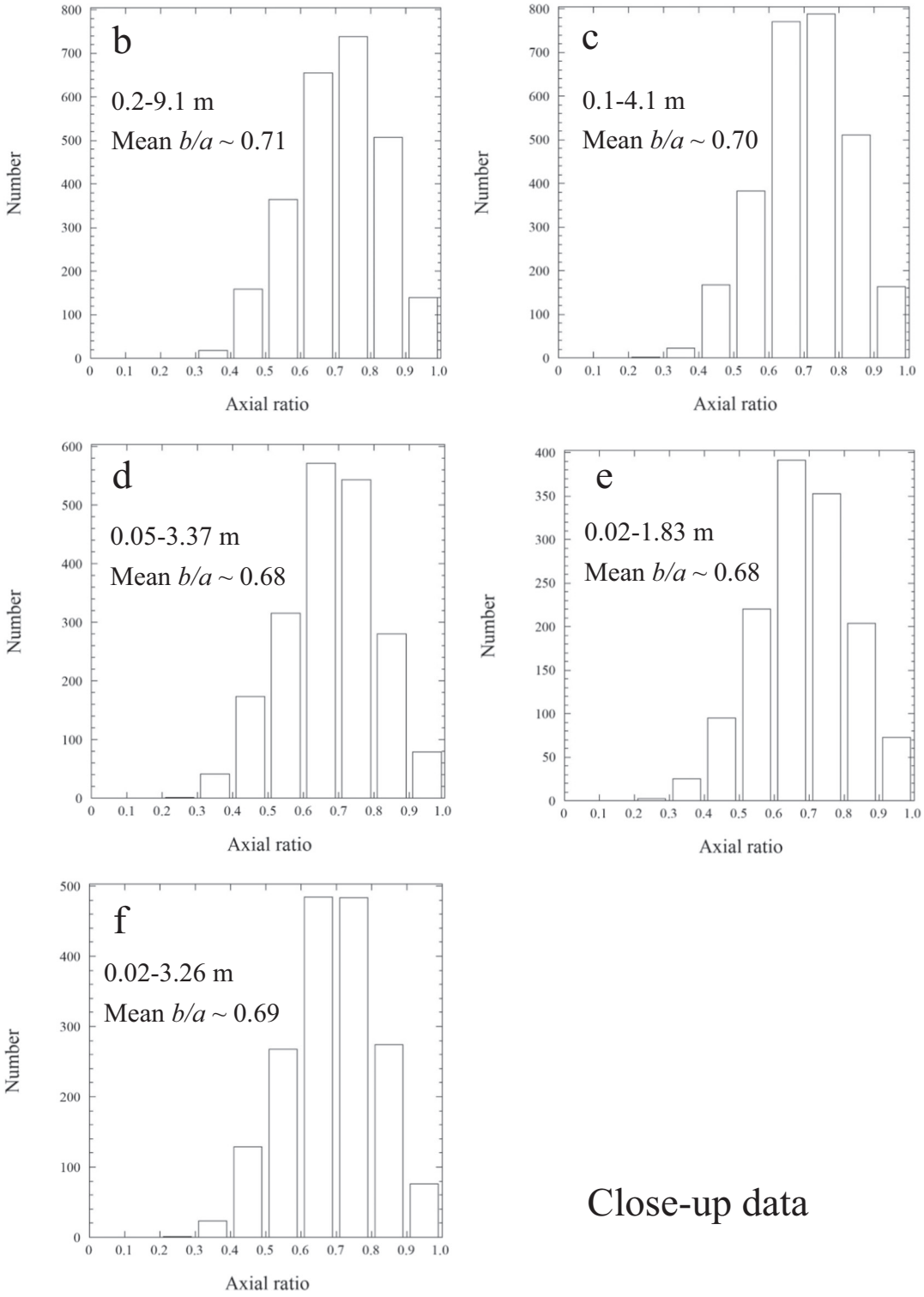

Fig. 8. Histograms of apparent axial ratios (b/a) of the boulders on close-up images, which are the same data presented in Fig. 5. The size range and mean b/a ratios of small boulders (including cobbles and pebbles) are indicated.

4. Discussion

4.1. Comparison with other asteroids

Our observations suggest that most boulders on Ryugu are likely to be fragments from a catastrophic disruption rather than from impact cratering. In order to better understand this formation scenario, we now compare our observations with other asteroids visited by spacecraft.

Michikami et al. (2008) concluded that most boulders on Itokawa were produced by the disruption of the larger parent body of this object. There are three observation results for Itokawa. (1) The relative size of the largest boulder to the largest crater is higher compared with other asteroids previously observed by spacecraft, (2) the boulders are uniformly spread over the entire surface except for a smooth area, independent of the locations of craters, and (3) the number density of the boulders is higher than on other asteroid, such as Eros. These three

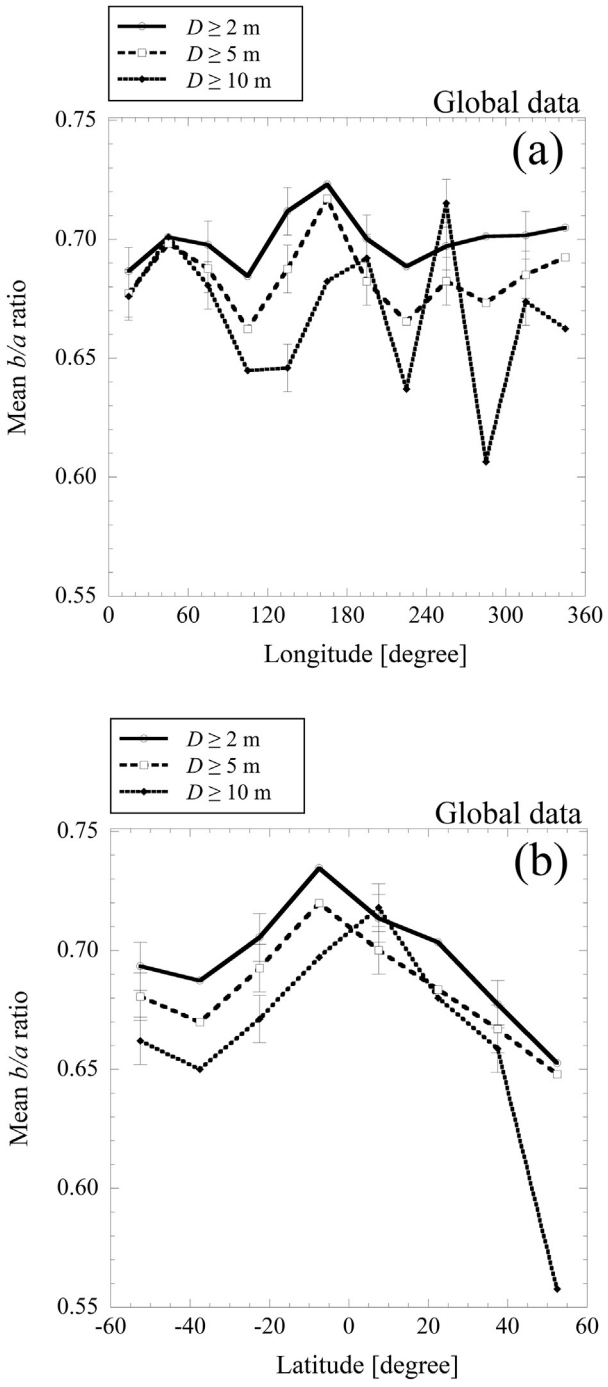

Fig. 9. (a) Mean axial ratio (b/a) of the boulders with three different size range ($\geq$2 m (total counted), $\geq$5 m and $\geq$10 m in diameter) as a function of longitude for Ryugu. Error bars are restricted to only a few points to improve legibility.
(b) Mean axial ratio (b/a) of the boulders with three different size range ($\geq$2 m (total counted), $\geq$5 m and $\geq$10 m in diameter) as a function of latitude for Ryugu. The error bars are given only for a few points to make the figure legible.

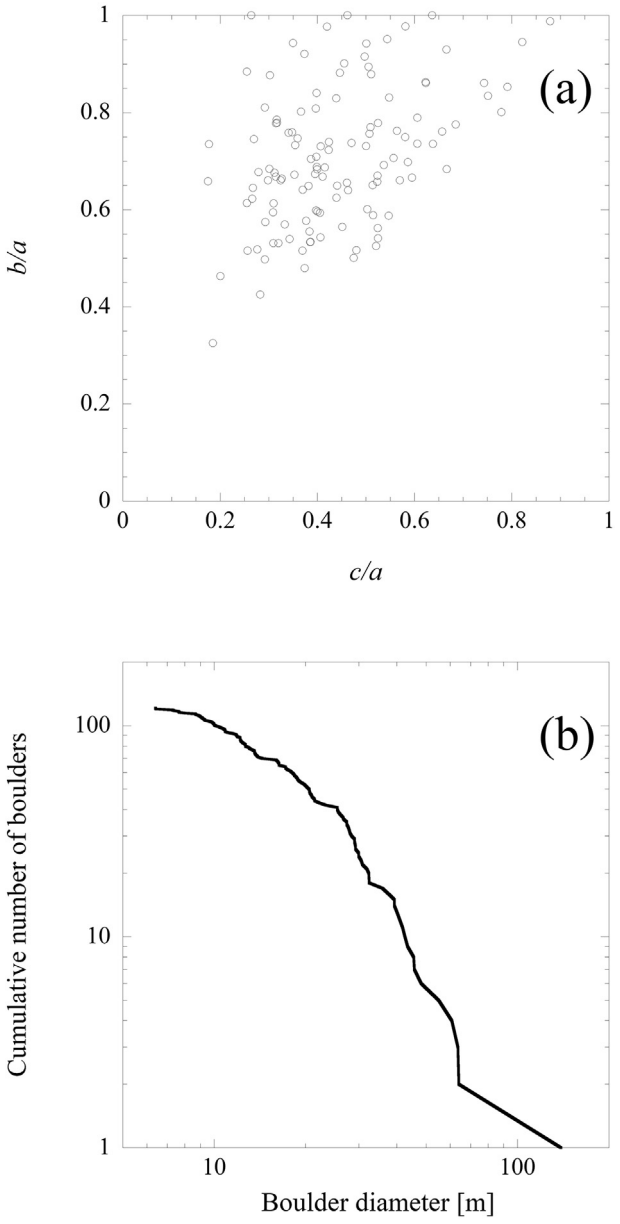

Fig. 10. (a) Shape distributions of 121 arbitrarily selected boulders acquired from a few hundred images on 20th July 2018. The mean b/a and c/a ratios are 0.71 and 0.44, respectively.
(b) Size distribution of 121 arbitrarily selected boulders.

observations also apply to Ryugu (and possibly to Bennu). However, with regard to observation (3), the number density of boulders smaller than 10 m in diameter on Ryugu is lower than on Itokawa, while reverse is true for boulders larger than 10 m. Therefore, on Ryugu, in order to put the volume of the boulders in relation to the total crater volume, we need to investigate the relationship between the total volume of the boulders and the total volume of the ejecta originating from craters.

Nearly 30 craters > 20 m in diameter, including crater candidates, are found on Ryugu (Sugita et al., 2019; Cho et al., 2019; Morota et al., 2019). The total volume of the excavated material of these craters can be estimated to be ~2.69×10^6 m^3, assuming that the excavated volume is half that of the crater volume - this method is also used by Thomas et al. (2001) and Michikami et al. (2008). The crater volume, V, is given by $V \sim 0.07\ D_c{}^3$, where D_c is the apparent crater diameter. The total calculated volume of observed boulders with diameters of 5 to 140 m is ~2.54×10^6 m^3, assuming the heights are half the diameter (the mean horizontal dimension). On Ryugu, the total volume of boulders reaches ~94% of the excavated volume of these craters. This percentage is considerably greater than on Eros (~0.4%; Thomas et al., 2001), the Moon (~5%; Cintala et al., 1982), Toutatis (10%; Jiang et al., 2015) and even Itokawa (~25%; Michikami et al., 2008). Note that, although accurate data on Bennu's craters and boulders have not yet been disseminated, the percentage on Bennu is considered to be smaller than on Ryugu. This is because, as indicated before, at

$28.2\,km^{-2}$, the number density of large boulders ≥ 20 m on Bennu is only half the number density of $\sim 50\,km^{-2}$ on Ryugu, while the power-index of -2.9 for the boulder size distribution on Bennu is similar to the power index of -2.65 on Ryugu. In addition, the cumulative crater frequency (km^{-2}) on Bennu appears to be higher than on Ryugu (see Fig. 3d in Walsh et al., 2019 and Fig. 2E in Sugita et al., 2019). Thus, the extremely high percentage of the total volume of boulders with respect to the total excavated crater volume on Ryugu strongly supports that the boulders on the surface of Ryugu cannot solely be the products of impact cratering.

Ryugu's high boulder abundance may imply the existence of a special mechanism. In general, for S-type asteroids previously visited by spacecraft, the number density of boulders appears to decrease with increasing asteroid size: the number densities of the boulders > 20 m on Itokawa ($0.535 \times 0.294 \times 0.209$ km), Toutatis ($\sim 4.6 \times 2.3 \times 1.9$ km) and Eros ($34 \times 11 \times 11$ km) are $\sim 25\,km^{-2}$ (Mazrouei et al., 2014), $\sim 17\,km^{-2}$ (Jiang et al., 2015), and $\sim 2\,km^{-2}$ (Thomas et al., 2001), respectively. However, the number density ($\sim 50\,km^{-2}$) of 20-m boulders on Ryugu ($1.04 \times 1.02 \times 0.88$ km) is greater than on Itokawa although Ryugu is larger than Itokawa. A similar tendency is also observed on carbonaceous asteroid Bennu. Here, the number density of $28.2\,km^{-2}$ for 20-m boulders is slightly larger than on Itokawa, although Bennu is larger ($0.565 \times 0.536 \times 0.498$ km; Lauretta et al., 2019) than Itokawa.

We attribute this to the fact that Ryugu and Bennu are a C-type and a carbonaceous asteroid, whereas the examples above are S-type asteroids. Carbonaceous chondrites, the main material constituents of C-type asteroids, are less strong than ordinary chondrites, which come from S-type asteroids (e.g. Popova et al., 2011). If the material is structurally weak, a large amount of ejecta tends to have lower velocities as indicated by laboratory impact experiments (e.g. Michikami et al., 2007) and can thus accumulate on the surface Therefore, on S-type asteroids, such as Itokawa, Toutatis and Eros, some excavated material, having higher velocities compared with C-type asteroids, may not be able to accumulate on the surface.

In another study, Jutzi et al. (2010) simulated the impact strength of a boulder with a high porosity and suggested that porosity can in fact lead to higher impact strength because it causes higher dissipation of impact energy by pore crushing. Ryugu and Bennu both have higher macroporosities - > 50% (Watanabe et al., 2019) and ~50% (Lauretta et al., 2019), respectively - than Eros (~20%; Wilkison et al., 2002) and Itokawa (~40%; Abe et al., 2006). Therefore, we cannot completely exclude the possibility of high impact-resistivity of boulders on C-type asteroids. However, in the case of Ryugu's boulders, the material is likely to be structurally weak because a large amount of material was ejected when the Hayabusa2 spacecraft touched down on the surface to collect the sample materials of Ryugu.

Considering observations (1) and (3) for Ryugu, these may indicate that Ryugu's parent body has experienced a heavier catastrophic disruption than Itokawa's. This is because the relative size of the largest boulder to the largest crater and the number density of the boulders on Ryugu are higher than those on Itokawa. For instance, many rugged boulders, which are typically covered with many rows of quasi-parallel layers, are observed in close-up images (e.g. Sugita et al., 2019). Although some rugged boulders are observed on Itokawa (e.g. Nakamura et al., 2008; Noguchi et al., 2010), the number of rugged boulders on Ryugu (and possibly on Bennu) is significantly greater than on Itokawa. A rugged surface means that the surface area per unit volume of the boulder is large, i.e. the surface energy during the formation is large. These boulders might have experienced high impact energy during their formation.

Of course, a possibility of boulder erosion by subsequent impact and/or thermal fatigue by the day-night temperature cycles on asteroid surfaces (Delbo et al., 2014; Molaro et al., 2015) cannot be ruled out. However, we consider this possibility to be low because, if erosion occurs, the production of many finer particles and pebbles should result in a steeper size distribution of boulders. Besides, several close-up images illustrate that the minimum size (~cm) of particles forming the regolith layers on Ryugu appears to be larger than that on Itokawa (Watanabe et al., 2019), and the number densities of small boulders are somewhat smaller than those on Itokawa. This may indicate that boulders on Ryugu have not evolved through erosion. Another explanation for the ruggedness of boulders is that their texture is heterogeneous. Sugita et al. (2019) suggest that the surface materials are a mixture of materials originating from various locations of its parent body. In any case, further investigation of the formation of rugged boulders is required.

4.2. Comparison with other observational results of Ryugu

Our observations of Ryugu indicate that the number density of boulders larger than 5 m is lower in the equatorial region than at higher latitudes, while the apparent mean b/a ratio has a higher peak in the equatorial region. On the other hand, there is only very little dependence of the apparent mean b/a ratios on longitude direction, although the number density of boulders is somewhat different on eastern and western sides. In order to explore possible formation and/or evolution processes of boulders in the equatorial region, we now compare our boulder counting results with other observation results, such as Ryugu's shape, crater, and surface features derived from ONC color observations and the Near-Infra Red Spectrometer (NIRS3). We also take Itokawa's and Bennu's boulders into account as necessary.

4.2.1. Lower number density of boulders in the equatorial region

Ryugu has an equatorial ridge considered to consist of mechanically unconsolidated materials (Sugita et al., 2019). The equatorial aspect ratio is as large as 0.98 (Watanabe et al., 2019). According to Watanabe et al. (2019) and Hirabayashi et al. (2019), the global material homogeneity, the constant surface slope between the equator and mid-latitude and the results of their numerical simulations indicate that the top-shape of Ryugu was produced by rotation-induced deformation as a result of a short spin period during either the early re-accumulation stage and/or a later stage due to quasi-static rotational acceleration. In other words, these observational results suggest that at a some point in its past, Ryugu rotated much faster, the resultant strong centrifugal force causing mass movement towards the equator (by convection from the interior of Ryugu or surface landslides), resulting in the formation of an equatorial ridge (Watanabe et al., 2019; Sugita et al., 2019; Hirabayashi et al., 2019). For instance, the regional variation in visible and NIR reflectance is within 15%, suggesting efficient surface mixing processes (Watanabe et al., 2019; Sugita et al., 2019). Besides, Ryugu does not have smooth areas with low boulder abundance as seen on Itokawa. This observation may indicate that the global uniform migration of unconsolidated materials occurs on Ryugu instead of local migration seen in the smooth area on Itokawa.

According to Sugita et al. (2019), the existence of unconsolidated materials is also observed from the crater geomorphology. Evidence for wall slumping is seen within some craters, indicating the presence of loose material. The craters on Ryugu do not have flat floors. This means that the craters consist of materials of similar strength (perhaps, unconsolidated materials) up to their depths. In particular, the lack of craters smaller than 100 m may indicate the presence of a crater obliteration mechanism, such as seismic shaking with unconsolidated materials.

As direct evidence for migration, there are many imbricated boulders near the equator. Such imbrication is clearly produced by landslides on the surface (Sugita et al., 2019). Although the direction of past migration is considered to be from high latitudes to the equatorial ridge, the direction of recent migration is from the equatorial ridge towards the topographic lows at higher latitudes, corresponding to the current geopotential of Ryugu (Sugita et al., 2019). As evidence of the recent migration, the general spectral slope from b-band (0.48 μm) to x-

band (0.86 μm) shows that the surface on the equatorial ridge has a bluer spectral slope, which implies the exposure of fresh surface material (Sugita et al., 2019). In any case, we think it is reasonable to assume that the migration of unconsolidated materials must have occurred on Ryugu's surface.

In general, particles smaller in size have higher mobility due to their lower friction angle. By contrast, larger boulders cannot move easily and some boulders are stuck at the surface owing to their larger friction angle (e.g. Miyamoto et al., 2007; Michikami et al., 2010). In the equatorial region, a large amount of smaller particles (including cobbles and pebbles) which migrated from higher latitudes in the past would still exist, burying themselves and some boulders. As a result, the number density of boulders in the equatorial region would decrease, and consequently the slope (the power-index) of the size distribution of small boulders decreases with decreasing boulder size.

Recent studies on Bennu strongly support the above scenario. The shape of Bennu is very similar to that of Ryugu and is consistent with spin-induced failure at some point in its past (Scheeres et al., 2019). On Bennu, material movement is observed and some boulders are partially buried by smaller particles (Walsh et al., 2019). As mentioned before, Bennu's power-index of boulder size distribution is similar to Ryugu's. Moreover, DellaGiustina et al. (2019) suggested that smaller particles preferentially migrate away from higher latitudes, resulting in the relative deficiency of larger boulders in the equator.

4.2.2. Higher peak in the mean b/a ratio of boulders in the equatorial region

It may be difficult to determine the cause of the difference between the equatorial region and higher latitudes in the mean b/a ratio of boulders because the data available at the time of writing are insufficient. However, in this sub-section, one possible scenario is introduced based on the idea of Michikami et al. (2010).

Michikami et al. (2010), who investigated the shape distributions of boulders on Itokawa and Eros, propose that the actual shape distribution of the boulders on any asteroid is similar to laboratory impact fragments. We believe this study underpins their hypothesis, as shown by the following three observational results.

(i) In laboratory impact experiments, fragment shapes from catastrophic disruptions have been found to behave similarly, independent of various experimental conditions and target materials. Recent studies show that this result has been found to be valid for fragments ranging from several tens of microns to several cm (Michikami et al., 2016, 2018).
(ii) Although only limited data on boulders whose three-axial lengths have been measured are available, the mean b/a and c/a ratios of boulders on Itokawa (Michikami et al., 2016) and Ryugu in this study are similar to laboratory impact fragments. The sizes of these boulders, which are considered to be impact fragments from their parent body, range from several meters to several tens of meters.
(iii) The mean b/a ratios of small- and fast-rotating asteroids, i.e. those with a diameter $<$ 200 m and a rotation period $<$ 1 h, which are considered to be monolith bodies, are similar to laboratory impact fragments (Michikami et al., 2010).

These three observational results strongly suggest that fragment shapes from catastrophic disruptions are independent of their sizes - at least on scales up to 100 m. The theoretical interpretation for this regularity of fragment shapes is recently given by Kadono et al. (2018).

Note that we do not rule out the possibility that the boulders on Ryugu are actually more elongated than predicted by laboratory-scale collision experiments. However, in light of observation (ii), we consider this to be unlikely.

The existence of a large amount of smaller particles and their mobility may affect the apparent mean b/a ratios of boulders in the equatorial region. We consider boulders to be fragments observed on the asteroid's surface. Assuming that the *actual* shape distribution of the boulders on Ryugu is similar to laboratory impact fragments, then the deviation from this distribution of the *apparent* b/a ratios of boulders observed could be indicative of a preferred orientation of the boulders, namely that their c axes are not perpendicular to the asteroid surface (On Itokawa, the orientations of the a axis of most boulders were observed to be parallel to the asteroid surface. Only the orientations of the c axis (or the b axis) would be somewhat random.)

As mentioned before, in the case of Ryugu shown in Fig. 9b, the apparent mean b/a ratios of boulders larger than 5 m in higher latitudes are slightly smaller than the ratios in laboratory impact fragments, i.e. the boulder shapes tend to be more elongated. This may imply that some boulders in higher latitudes are stuck on the surface of Ryugu due to their larger friction angle and remain at their original orientations - for instance, in the case of Itokawa, the large boulder called pencil is clearly stuck on the surface due to its larger friction angle (Saito et al., 2006). In the equatorial region on the other hand, the apparent mean b/a ratios of boulders larger than 5 m are similar to those of laboratory impact fragments. This may be caused by migration of many small particles in the equatorial region. This suggests that small particles might push and vibrate larger boulders in the equatorial region during the migration of small particles and as a result the c axes of most boulders become perpendicular to the surface owing to gravitational stability. On Eros for instance, the mean b/a ratios of boulders are similar to laboratory impact fragments (Michikami et al., 2010). Almost all boulders on Eros would have been re-orientated after their accumulation by global vibration (e.g. Richardson et al., 2005) and then the c axes of all boulders would be oriented perpendicular to the surface because the gravity of Eros is considerably larger than that of Itokawa (Michikami et al., 2010). After all, reorientations of boulders would occur in the equatorial region of Ryugu.

5. Conclusions

We have identified ~4400 boulders $\geq$ 5 m in mean horizontal dimension on the entire surface (~2.7 km^2) of Ryugu by analyzing images taken by ONC onboard Hayabusa2 at an altitude of about 6.5 km (resolutions ~0.65 m/pixel) on 20th July 2018. The size of the largest boulder called “Otohime” is 140 m, which is relatively large compared with the largest crater (300 m) on Ryugu. The number density of boulders $\geq$ 20 m on Ryugu is ~50 km^{-2}, which is twice as large as on Itokawa (or Bennu). The ratio of the total volume of boulders $\geq$ 5 m to the total excavated volume of craters $>$ 20 m on Ryugu can be estimated to be ~94%. This ratio is significantly larger than other asteroids such as Eros (~0.4%; Thomas et al., 2001), Toutatis (10%; Jiang et al., 2015) and Itokawa (~25%; Michikami et al., 2008). Boulders on Ryugu appear to be uniformly distributed over the entire surface, although there are slight differences in distribution with longitude and latitude. Together, these observational results suggest that most boulders were produced by the disruption of the Ryugu's larger parent body, as has been described in previous papers (Watanabe et al., 2019; Sugita et al., 2019).

The cumulative boulder size distribution on the entire surface has a power-index of -2.65 ± 0.05, which is less steep compared with other asteroids visited by spacecraft. This implies that some boulders are buried in a regolith layer consisting of finer particles. We also measured small boulders, cobbles and pebbles in close-up images taken at an altitude of 67–620 m (resolutions 0.7–6 cm/pixel) on 21th September 2018. The results show that the slope (power-index) of the cumulative size distribution gradually decreases with boulder size (e.g. the power-index is -2.01 ± 0.06 for boulders of 0.1–4.1 m in size and -1.65 ± 0.05 for boulders of 0.02–3.26 m, respectively), supporting the idea that smaller boulders are buried in the regolith layer. Several close-up images directly indicate some buried boulders.

The shape distribution of boulders on Ryugu shows that the apparent mean b/a ratio of boulders larger than 5 m is 0.68, which is similar to the ratios of laboratory impact fragment which lie in the

range 0.70–0.74 (Fujiwara et al., 1978; Capaccioni et al., 1984, 1986; Michikami et al., 2016, 2018). Moreover, the apparent mean axial b/a ratios of boulders ≥ 5 m in the equatorial region range from 0.70 to 0.72, slightly larger values than are found in higher latitudes (0.65–0.69).

From the boulder counting and other observational results on Ryugu, we propose that migration of small particles (including cobbles and pebbles) occurred from higher latitudes to the equatorial region during the formation of the equatorial ridge, and a large amount of these small particles still exists in the equatorial region (although the direction of recent migration is from the equatorial ridge towards the topographic lows at higher latitudes, corresponding to the current geopotential of Ryugu). These small particles bury themselves and some boulders, and as a result the number density of the boulders in the equatorial region is lower than at higher latitudes. Moreover, during migration these small particles may push and vibrate boulders in the equatorial region, resulting in the boulders "lying down" on the surface, i.e. with their c axes predominantly orientated perpendicular to the surface owing to gravitational stability. As a result, the apparent mean axial b/a ratio of boulders is higher in the equatorial region than higher latitudes.

Acknowledgements

We would like to thank all members of Hayabusa2 mission team for their support of the data acquisition. We thank S. Mazrouei and O.S. Barnouin for providing data of Itokawa. This paper was significantly improved by the comments from two anonymous reviewers. M.H. acknowledges support from Auburn University's Department of Aerospace Engineering. A.H. is supported by STFC, grant no. ST/S001271/1. C.M.E. is supported by the NASA Hayabusa2 Participating Scientist program. The research was supported by the Japan Society for the Promotion of Science (JSPS) KAK- ENHI (Grant Number 17H01175) and Core-to-Core program "International Network of Planetary Sciences."

References

Abe, S., Mukai, T., Hirata, N., et al., 2006. Mass and local topography measurements of Itokawa by Hayabusa. Science 312, 1344–1347.
Bart, G.D., Melosh, H.J., 2010. Distributions of boulders ejected from lunar craters. Icarus 209, 337–357.
Belton, M.J.S., Chapman, C.R., Klaasen, K.P., et al., 1996. Galileo's encounter with 243 Ida: an overview of the imaging experiment. Icarus 120, 1–19.
Capaccioni, F., Cerroni, P., Coradini, M., et al., 1984. Shapes of asteroids compared with fragments from hypervelocity impact experiments. Nature 308, 832–834.
Capaccioni, F., Cerroni, P., Coradini, M., et al., 1986. Asteroidal catastrophic collisions simulated by hypervelocity impact experiments. Icarus 66, 487–514.
Cho, Y., Morota, T., Kanamaru, M., et al., 2019. Spatial distribution and morphology of craters on Ryugu: implications for surface processes on the C-type asteroid. Lunar Planet. Sci. Conf. 50 (2132).
Cintala, M.J., Garvin, J.B., Wetzel, S.J., 1982. The distribution of blocks around a fresh lunar mare crater. Proc. Lunar Planet. Sci. Conf. 13, 100–101.
Clauset, A., Shalizi, C.R., Newman, M.E.J., 2009. Power-law distributions in empirical data. SIAM Rev. 51, 661–703.
Delbo, M., Libourel, G., Wilkerson, J., et al., 2014. Thermal fatigue as the origin of regolith on small asteroids. Nature 508, 233–236.
DellaGiustina, D.N., Emery, J.P., Golish, D.R., et al., 2019. Properties of rubble-pile asteroid (101955) Bennu from OSIRIS-REx imaging and thermal analysis. Nat. Astron. 3, 341–351. https://doi.org/10.1038/s41550-019-0731-1.
Ernst, C.M., Barnouin, O.S., Daly, R.T., the Small Body Mapping Tool Team, 2018. The small body mapping tool (SBMT) for accessing visualizing, and analyzing spacecraft data in three dimensions. Lunar Planet. Sci. Conf. 49 (2083).
Fujiwara, A., Kamimoto, G., Tsukamoto, A., 1978. Expected shape distribution of asteroids obtained from laboratory impact experiments. Nature 272, 602–603.
Fujiwara, A., Kawaguchi, J., Yeomans, D.K., et al., 2006. The rubble-pile asteroid Itokawa as observed by Hayabusa. Science 312, 1330–1334.
Hartmann, W.K., 1969. Terrestrial, lunar, and interplanetary rock fragmentation. Icarus 10, 201–213.
Hirabayashi, M., Tatsumi, E., Miyamoto, H., et al., 2019. The western bulge of 162173 Ryugu formed as a result of a rotationally driven deformation process. Astrophys J Lett 874 (L10). https://doi.org/10.3847/2041-8213/ab0e8b. 6pp.
Hirata, N., Barnouin-Jha, O.S., Honda, C., et al., 2009. A survey of possible impact structures on 25143 Itokawa. Icarus 200, 486–502.
Huang, J., Ji, J., Ye, P., et al., 2013. The ginger-shaped asteroid 4179 Toutatis: new observations from a successful flyby of Chang'e-2. Sci. Rep. 3, 3411.
Jiang, Y., Ji, J., Huang, J., et al., 2015. Boulders on asteroid Toutatis as observed by Chang'e-2. Sci. Rep. 5, 16029.
Jutzi, M., Michel, P., Benz, W., et al., 2010. Fragment properties at the catastrophic disruption threshold: the effect of the parent body's internal structure. Icarus 207, 54–65.
Kadono, T., Tanigawa, T., Kurosawa, K., et al., 2018. Correlation between fragment shape and mass distributions in impact disruption. Icarus 309, 260–264.
Kameda, S., Suzuki, H., Takamatsu, T., et al., 2017. Preflight calibration test results for optical navigation camera telescope (ONC-T) onboard the Hayabusa2 spacecraft. Space Sci. Rev. 208, 17–31.
Lauretta, D.S., DellaGiustina, D.N., Bennett, C.A., et al., 2019. The unexpected surface of asteroid (101955) Bennu. Nature 568, 55–60. https://doi.org/10.1038/s41586-019-1033-6.
Lee, P., Veverka, J., Thomas, P.C., et al., 1996. Ejecta blocks on 243 Ida and on other asteroids. Icarus 120, 87–105.
Mazrouei, S., Daly, M.G., Barnouin, O.S., et al., 2014. Block distribution on Itokawa. Icarus 229, 181–189.
Michel, P., Richardson, D.C., 2013. Collision and gravitational reaccumulation: possible formation mechanism of the asteroid Itokawa. Astron. Astrophys. 554, 1–4.
Michikami, T., Moriguchi, K., Hasegawa, S., Fujiwara, A., 2007. Ejecta velocity distribution for impact cratering on porous and low strength targets. Planet Space Sci 55, 70–88.
Michikami, T., Nakamura, A.M., Hirata, N., et al., 2008. Size-frequency statistics of boulders on global surface on asteroid 25143 Itokawa. Earth Planets Space 60, 13–20.
Michikami, T., Nakamura, A.M., Hirata, N., 2010. The shape distribution of boulders on asteroid 25143 Itokawa: comparison with fragments from impact experiments. Icarus 207, 277–284.
Michikami, T., 2012. Proceeding of the Space Plasma Workshop for 2011. no. 19 ISAS/JAXA (Japanese).
Michikami, T., Hagermann, A., Kadokawa, T., et al., 2016. Fragment shapes in impact experiments ranging from cratering to catastrophic disruption. Icarus 264, 316–330.
Michikami, T., Kadokawa, T., Tsuchiyama, A., et al., 2018. Influence of petrographic textures on the shapes of impact experiment fine fragments measuring several tens of microns: comparison with Itokawa regolith particles. Icarus 302, 109–125.
Miyamoto, H., Yano, H., Scheeres, D.J., et al., 2007. Regolith migration and sorting on asteroid Itokawa. Science 316, 1011–1014.
Molaro, L.J., Byrne, S., Langer, A.S., 2015. Grain-scale thermoelastic stresses and spatiotemporal temperature gradients on airless bodies, implications for rock breakdown. J. Geophys. Res. Planets 120, 255–277.
Morota, T., Cho, Y., Kanamaru, M., et al., 2019. Timescale of reddening process of the Ryugu surface based on the crater size-frequency distribution. Lunar Planet. Sci. Conf. 50, 2132.
Nakamura, A.M., Michikami, T., Hirata, N., et al., 2008. Impact process of boulders on the surface of asteroid 25143 Itokawa—fragments from collisional disruption. Earth Planets Space 60, 7–12.
Noguchi, T., Tsuchiyama, A., Hirata, N., et al., 2010. Surface morphological features of boulders on asteroid 25143 Itokawa. Icarus 206, 319–326.
Popova, O., Borovicka, J., Hartmann, W.K., et al., 2011. Very low strengths of interplanetary meteoroids and small asteroids. Meteor Planet. Sci. 46, 1525–1550.
Richardson, J.E., Melosh, H.J., Greenberg, R.J., O'Brien, D.P., 2005. The global effects of impact-induced seismic activity on fractured asteroid surface morphology. Icarus 179, 325–349.
Saito, J., Miyamoto, H., Nakamura, R., et al., 2006. Detailed images of asteroid 25143 Itokawa from Hayabusa. Science 312, 1341–1344.
Scheeres, D.J., McMahon, J.W., French, A.S., et al., 2019. The dynamic geophysical environment of (101955) Bennu based on OSIRIS-REx measurements. Nat. Astron. 3, 352–361. https://doi.org/10.1038/s41550-019-0721-3.
Sugita, S., Honda, R., Morota, T., et al., 2019. The geomorphology, color, and thermal properties of Ryugu: implications for parent-body processes. Science 364. https://doi.org/10.1126/science.aaw0422.
Tancredi, G., Roland, S., Bruzzone, S., 2015. Distribution of boulders and the gravity potential on asteroid Itokawa. Icarus 247, 279–290.
Thomas, P.C., Veverka, J., Robinson, M.S., Murchie, S., 2001. Shoemaker crater as the source of most ejecta blocks on the asteroid 433 Eros. Nature 413, 394–396.
Veverka, J., Robinson, M., Thomas, P., et al., 2000. NEAR at Eros: imaging and spectral results. Science 289, 2088–2097.
Walsh, K.J., Jawin, E.R., Ballouz, R.-L., et al., 2019. Craters, boulders and regolith of (101955) Bennu indicative of an old and dynamic surface. Nat. Geosci. 12, 242–246. https://doi.org/10.1038/s41561-019-0326-6.
Watanabe, S., Hirabayashi, M., Hirata, N., et al., 2019. Hayabusa2 arrives at the carbonaceous asteroid 162173 Ryugu—a spinning top–shaped rubble pile. Science 364, 268–272. https://doi.org/10.1126/science.aav8032.
Wentworth, C.K., 1922. A scale of grade and class terms for clastic sediments. J. Geol. 30, 377–392.
Wilkison, S.L., Robinson, M.S., Thomas, P.C., et al., 2002. An estimate of Eros's porosity and implications for internal structure. Icarus 155, 94–103.